Polymer Chemistry

Accepted Manuscript

ROYAL SOCIETY OF CHEMISTRY

www.rsc.org/polymers

Journal Name

RSCPublishing

ARTICLE

Ultra bright Red AIE Dots for Cytoplasm and Nuclear Imaging

Cite this: DOI: 10.1039/xoxxoooooox

Zilong Wang [a], Lulin Yan[a], Lei Zhang[b], Yujue Chen[b], Hui Li [a], Jibo Zhang [a], Yan Zhang[a], Xing Li[a], Bin Xu[a]*, Xueqi Fu[b], Zaicheng Sun[c], Wenjing Tian [a]*

Received ooth January 2012,
Accepted ooth January 2012

DOI: 10.1039/xoxxoooooox

www.rsc.org/

An aggregation-induced emission (AIE) molecule (2-(2,6-bis((E)-2-(5-(N,N- bis(4-((E)-2-(10-((E)-4-(diphenylamino)styryl)anthracen-9-yl)vinyl)phenyl)aniline-4-yl)thiophen-2-yl)vinyl)-4H-pyran-4-ylidene)malononitrile) (TPA-AN-TPM) with near-infrared emission was synthesized by coating disc-like red emission fluorophore with propeller-shaped AIE fluorophore. The ultrabright red AIE dots TPA-AN-TPM@Ps-PVPs (TPA-AN-TPM in poly(styrene)-poly(4-vinylpyridine) nanoparticles) with the absolute quantum yield of 12.9% were fabricated by using the AIE molecule TPA-AN-TPM as the core and one biocompatible polymer Ps-PVP as the encapsulation matrix. The AIE dots are mono-dispersed with the average diameter of 25 nm, and stable in aqueous suspension. In particular, the AIE dots can stain both cytoplasm and nuclei with a strong red fluorescent signal, and pose little toxicity to living cells.

Introduction

Fluorescent imaging of tissues has gained significant attention in recent years due to its high sensitivity, high resolution, and possibility to monitor biological phenomena in real time which enable the noninvasive study of gene expression, protein function, protein-protein interactions, and a large number of cellular processes.[1, 2]In general, the fluorescent imaging based on the traditional fluorescent dyes is restricted by the broad emission, limited emission per molecule and poor photostability of the fluorescent dyes. In order to overcome the above limitations, fluorescent imaging based on nanoparticles has been gradually developed.[2] Recently, some research about the fluorescent imaging based on nanoparticles, including dye-containing nanoparticles, quantum dots (QDs), upconversion nanoparticles, and gold nanoclusters have been reported.[3-6]In comparison to the nanoparticles from inorganic molecules, organic fluorescent nanoparticles are richer in variety and more compatible with living cells. And by controlling the fabrication conditions of the fluorescent nanoparticles, organic dots with good optical features, cellular retention time, superior cytocompatibility and fluorescent stability could be obtained.[7, 8] However, the emission of the traditional organic fluorescent molecules is weakened or annihilated in their aggregate states due to the aggregation-caused quenching (ACQ) effect. [9]

In 2001, a intriguing phenomenon, which is named as aggregation-induced emission (AIE), was reported by Tang's group.[10]The AIE fluorophores are non-emissive when they are well-dissolved in solution but become highly emissive upon aggregation due to the restriction of intramolecular rotations (RIR) that activates radiative decay channels. [11-15]And recently AIE dyes are applied to design highly fluorescent nanoparticles which have been widely applied in cell imaging.[16-20]

Fluorescent nanoparticles based on fluorophores with intense emission in the far red/near-infrared (FR/NIR) (650–900 nm) region have attracted much interest due to their low photodamage, deep tissue penetration and minimal auto-fluorescence from biological substrates in this wavelength range. [11-13]However, there are only limited reports [21-27]about red AIE fluorescent nanoparticles. The main reason is that, the AIE fluorophores are general propeller-shaped, non-planar and with several rotor constitutional units. [28]But red emission fluorophores are generally disc-like fused planar rings with extended conjugation or with strong dipoles stemmed from π-conjugated electron-donating and accepting groups.[29-31] This kind of molecular configuration make them highly susceptible to the concentration quenching due to the strong dipole–dipole interactions and/or intermolecular π–π interactions. As a result, the nanoparticles or solid films based on red emission fluorophores can usually offer weak emissions.[32]

Here, we present a strategy to design molecules with both AIE characteristics and red emission, coating disc-like red emission fluorophores with propeller-shaped AIE fluorophores. The outside AIE fluorophores could separate the inside large conjugated planes apart from each other in the aggregation state, thereby prevent the strong dipole–dipole interactions and π–π interactions, thus avoid the fluorescent quenching. Based on the above considerations, we synthesized an AIE active and

red emission molecule, (2-(2,6-bis((E)-2-(5-(N,N-bis(4-((E)-2-(10-((E)-4-(diphenylamino)styryl)anthracen-9-yl)vinyl)phenyl) aniline-4-yl)thiophen-2-yl)vinyl)-4H-pyran-4ylidene) malononitrile) (TPA-AN-TPM) (shown in Scheme 1), by combining the electron-donating group (4-bromo-N,N-bis(4-((E)-2-(10-((E)-4-(diphenylamino)styryl)anthracen-9-yl)vinyl)phenyl)aniline) (TPA-AN-Br) (shown in Scheme 2) with the electron-withdrawing group 2-(2,6-dimethyl-4H-pyran-4- ylidene)malononitrile (TPM) (shown in Scheme 1) and fabricated the ultrabright red AIE dots TPA-AN-TPM@Ps-PVPs (TPA-AN-TPM in poly(styrene)-poly(4- vinylpyridine) nanoparticles) with the absolute quantum yield of 12.9% by using the AIE molecule TPA-AN-TPM as the core and one biocompatible polymer Ps-PVP as the encapsulation matrix. This red AIE dots with high fluorescent quantum yield can be applied effectively in cytoplasm and nucleus imaging.

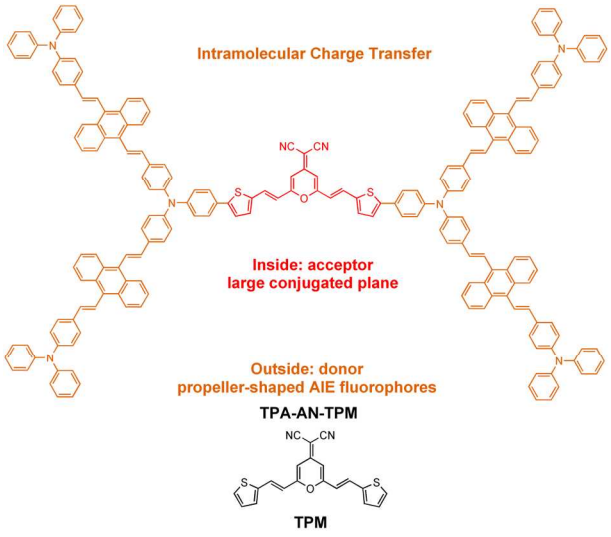

Scheme 1. Design strategy and chemical structure of TPA-AN-TPM. Chemical structure of TPM is also shown.

Results and Discussion

Synthesis of TPA-AN-TPM

TPA-AN-TPM was prepared according to the synthetic routes shown in Scheme 2. Compound 3 was synthesized by coupling 1 and 2 through Wittig-Horner reaction. Then TPA-AN-Br was synthesized through Wittig-Horner reaction between 4 and excess 3. The important intermediate 5 was synthesized by metathesis of the TPA-AN-Br's bromine atom for boronpinacolate. The desirable compound of TPA-AN-TPM was obtained with a yield of 56% by Suzuki coupling between 5 and 6 using tetrakis-(triphenylphosphane)palladium(0) (Pd(PPh3)4) as a catalyst in basic media. All compounds were characterized by standard spectroscopic methods, from which satisfactory analysis data corresponding to their molecular structures were obtained. The final product gives a $[M + H]^+$ peak at m/z 2733.221 (calcd: 2733.05) in the MALDI-TOF MS spectra (Figure S1, Supporting Information) for TPA-AN-TPM, confirming the formation of the expected adducts.

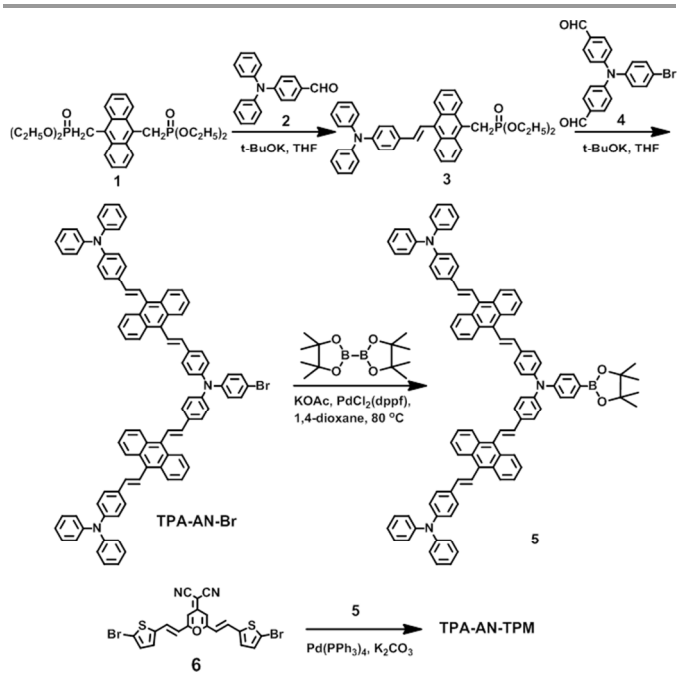

Scheme 2. Synthetic route to TPA-AN-TPM

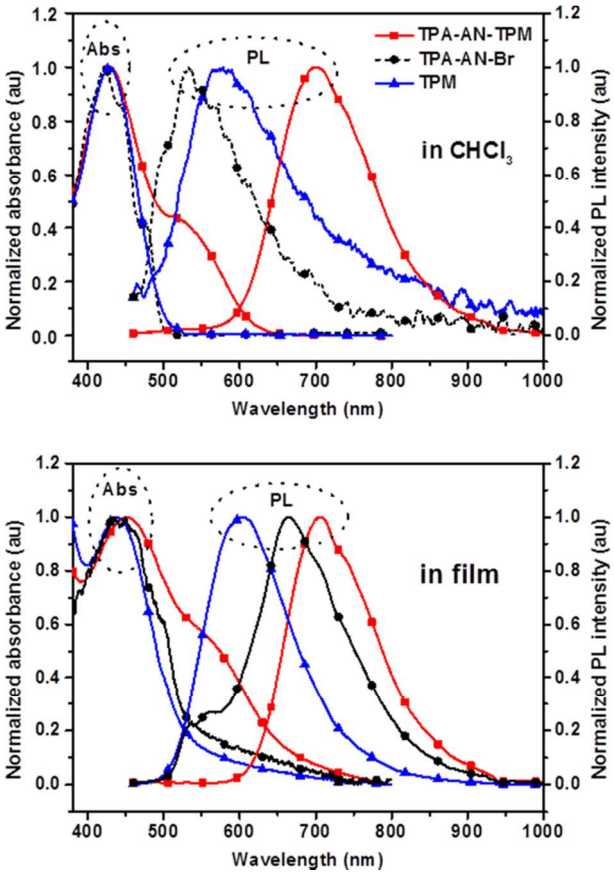

Figure 1. Normalized UV–vis absorption and PL emission spectra of TPA-AN-TPM and TPA-AN-Br in $CHCl_3$ and in film. The spectrum of TPM is also shown for comparison.

Photophysical Properties

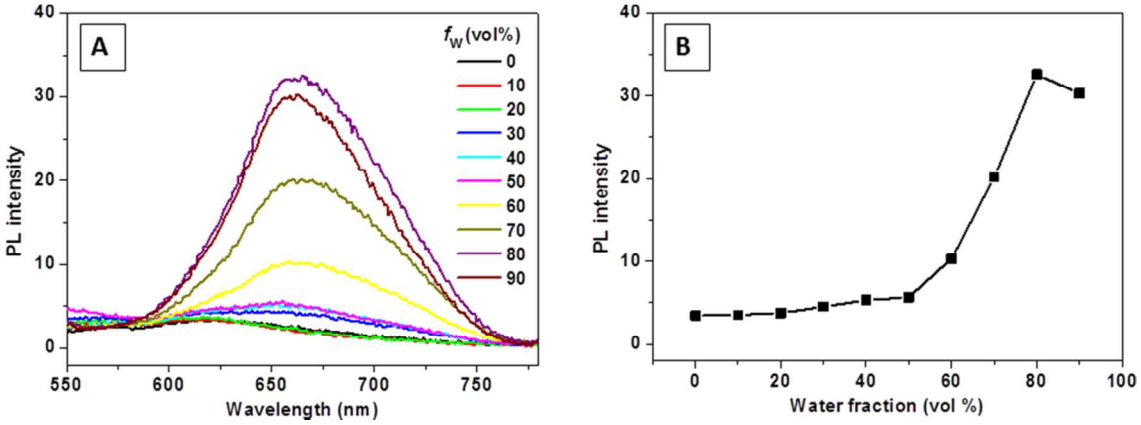

Figure 2.A) PL spectra of TPA-AN-TPM in CH_3CN/water mixtures with different water fractions (f_w);B) Plot of peak intensity of TPA-AN-TPM versus water fraction in the aqueous mixtures. [TPA-AN-TPM] = 10^{-5}M; λ_{ex} = 525 nm

Figure 1 shows the absorption and PL emission spectra of TPM, TPA-AN-Br and TPA-AN-TPM in solution. The maximum absorption peak of TPM and TPA-AN-Br located in 420nm and 429nm, respectively. And there are two absorption peaks (429 nm and 524 nm) in the absorption spectrum of TPA-AN-TPM. Comparing with the absorption spectrum of TPM, TPA-AN-Br and TPA-AN-TPM, we know that the peak at 429 nm is attributable to the absorption of the TPA-AN and TPM units, while the peak at 524 nm is attributable to the π–π* transition of the intramolecular charge transfer (ICT) state of TPA-AN-TPM. The PL emission peak of TPA-AN-TPM is in the near-infrared region (around 701nm) which is bathochromic compared to that of TPM(533nm) and TPA-AN-Br(577nm) due to the formation of the intramolecular charge transfer (ICT) state,33 and the ICT effect also leads to a large Stokes shift (~250 nm) for TPA-AN-TPM.

The UV–vis absorption and PL emission spectra of TPM, TPA-AN-Br, TPA-AN-TPM in film are also shown in Figure 1. The absorption of TPA-AN-TPM in the film is red shifted 38 nm, indicating that there is weak π–π interaction in the aggregation state because of the large size of the molecules and lots of noncoplanar 9,10-divinylanthracene segments. TPA-AN-TPM shows strong near-infrared emission peaked at 706 nm, which validates that TPA-AN-TPM molecule should be AIE active.

To further verify the AIE property of TPA-AN-TPM, the PL spectra of TPA-AN-TPM solution with different fraction of water is shown in Figure 2. The solutions of TPA-AN-TPM almost had no emission when the water fraction was less than 50 %. However, the fluorescence increased rapidly with the water fraction increasing from 50 % to 80 % due to the formation of TPA-AN-TPM nanoparticles with high water fractions. Unexpectedly, the fluorescent intensity decreased with the water fraction increasing over 80 %, which has been theorized that in the mixture with ‘‘high’’ water content, solute molecules quickly aggregated in a random way to form less emissive.[34, 35] Herein, there may be another reason that in the mixture with ‘‘high’’ water content, the solute molecules agglomerated into bigger nanoparticles and the inner molecules was shielded in some extent, resulting in the decrease of the fluorescent intensity of the mixture. The broadening of the emission peak in high water fractions suggests a more serious light scattering occurs, which is consistent with our conjecture. This phenomenon is also obvious for TPA-AN-Br whose AIE property is shown in Figure S2. The DLS analysis of TPA-AN-Br in THF/water mixtures (shown in Figure S2) suggests that the particle size is larger and with a much broader distribution when the water fraction increases to 90 %, which could be an evidence for our conjecture.

TPA-AN-TPM Encapsulated Polymeric Micelle

To explore the potential application of TPA-AN-TPM in bioimaging, we prepared AIE dots, TPA-AN-TPM@PS-PVP, by using TPA-AN-TPM loaded polymer micelle, where PS-PVP (molecular weight: 19K and 20K for PS chain and PVP chain, respectively) served as the coating layer. The preparation procedure and the structure of TPA-AN-TPM@PS-PVP are illustrated in Scheme S2. TPA-AN-TPM and PS-PVP were dissolved in a THF solution and stirred for 0.5 h to mix them well. Then a certain amount of dilute hydrochloric acid (pH = 2) was added at a rate of 0.5 mL/h. The poly (4-vinylpyridine) (PVP) chains would be protonated by hydrochloric acid, and became hydrophilic and stretched out into the water phase gradually. While the hydrophobic poly(styrene) (PS) chains and TPA-AN-TPM molecules would aggregate and entangle together into the core. After that, the THF was then removed by dialysis and the micelle nanoparticles were further purified by filtration through a 0.45 μm micro filter. For further research, we fabricated AIE dots with five different fluorogen loading amount (mass fractions of TPA-AN-TPM in the AIE dots: 2%, 4%, 6%, 8%, 10%) by changing the ratio of TPA-AN-TPM and PS-PVP. Precipitation occurred during the fabricating procedure when we used more fluorogen, so 10% may be the limit fluorogen loading amount. And the dots with 10% fluorogen loading amount served as a representative for properties measuring. The dots are stabilized in water phase because of the outer layer pyridine salt groups. The zeta

potential curve of the dots in aqueous suspension is shown in Figure S4, which indicates that the AIE dots are very stable for high Zeta potentials.

Figure 3A shows the transmission electron microscopy (TEM) image of TPA-AN-TPM@Ps-PVP (10 wt%). The morphology indicates that the prepared AIE dots (10 wt% mass fractions of fluorogen) are well shaped nanospheres with an almost uniform size around 25 nm. Dynamic light scattering (DLS) studies of the dots confirmed the monodisperse and uniform size by showing a narrow peak in the size distribution diagram and the volume average hydrodynamic diameters is 75.98 nm (distribution width 14.44nm), shown in Figure 3B. The size is somewhat larger than that measured by TEM due to the swelling of the TPA-AN-TPM@Ps-PVPs, the stretching of outer layer PVP chains in aqueous mixtures and the shrinkage under the high vacuum in the TEM chamber.

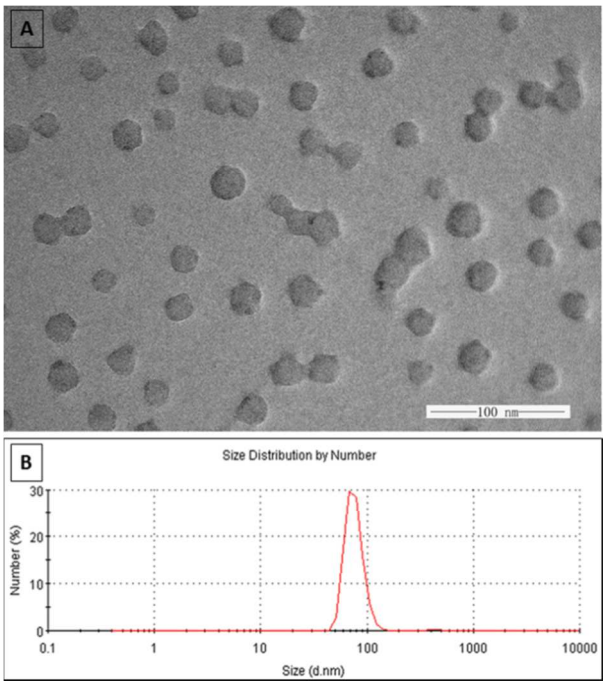

Figure 3.TEM image (A) and particle size distribution in aqueous media (B) of TPA-AN-TPM@Ps-PVPs.

Figure 4 shows the normalized absorption and emission spectra of TPA-AN-TPM@Ps-PVPs(with a 10 wt% TPA-AN-TPM loading) in water. The spectra are similar with those of TPA-AN-TPM in solution. But the emission peak is located at 643nm which is blue-shifted by 63 nm compared to that of TPA-AN-TPM in solution. From the structure analysis of DSA derivatives in our previous work,[36-40] the molecular conformation in crystalline state tend to more twisted than that of the optimized geometries in gas state, resulting in the lower conjugation of the molecule and the blue shifted emission in the aggregation state. The blue shifted emission of AIE dots hence may origin from the more twisted molecular configuration of TPA-AN-TPM in the AIE dots compared with that in the solution. The severely restricted intramolecular rotations of TPA-AN-TPM in the AIE dots also cause a surge in the emission intensity.

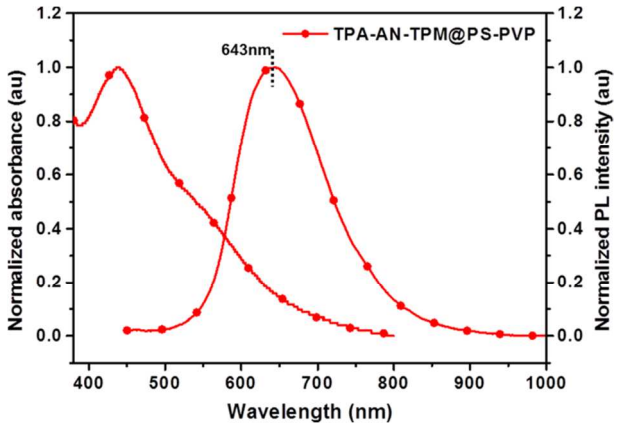

Figure 4. Normalized UV-vis absorption and PL emission spectra of TPA-AN-TPM@Ps-PVPs (with a 10 wt% TPA-AN-TPM loading) in water.

Figure 5A shows an image of the suspension of TPA-AN-TPM@Ps-PVPs and solution of TPA-AN-TPM as well as Ps-PVP which was taken upon exposure to the irradiation under a UV light of 365 nm. Figure 5B shows an image taken under laboratory lighting for comparison. The intense red light (643nm) emits from TPA-AN-TPM@Ps-PVPs under the UV illumination (the absolute quantum yield: 12.9%), whereas the dilute solutions of TPA-AN-TPM, and Ps-PVP almost have no light emission. When TPA-AN-TPM molecules are fixed in the polymer micelle, the restriction of the intramolecular rotations can block the non-radiative relaxation channel and populate the radiative decay, thus making the TPA-AN-TPM@Ps-PVPs highly luminescent. In addition, the fluorescent quantum yield of TPA-AN-TPM@Ps-PVPs increases rapidly with increasing fluorophore loading (Table S1), manifesting that TPA-AN-TPM does not suffer from the ACQ effect. The absolute quantum yield of TPA-AN-TPM@Ps-PVPs reaches a value of 12.9% at a fluorogen loading of 10 wt%，which is relatively high for the red AIE dots that have been reported. [24, 41]

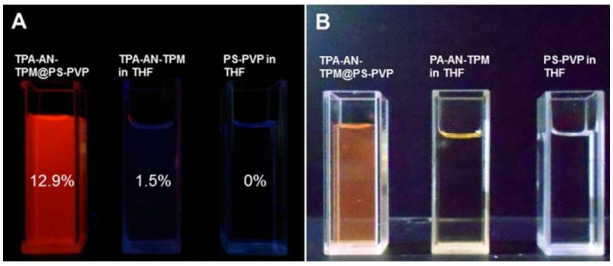

Figure 5. Suspension of TPA-AN-TPM@Ps-PVPs in water and solutions of TPA-AN-TPM as well as Ps-PVP in THF; photographs taken upon irradiation under laboratory lighting (B) and a UV light of 365 nm (A).The samples' quantum yields are labeled respectively.

Intracellular Imaging

The strong red emission, suitable size and good stability in water phase of TPA-AN-TPM@Ps-PVP prompted us to explore

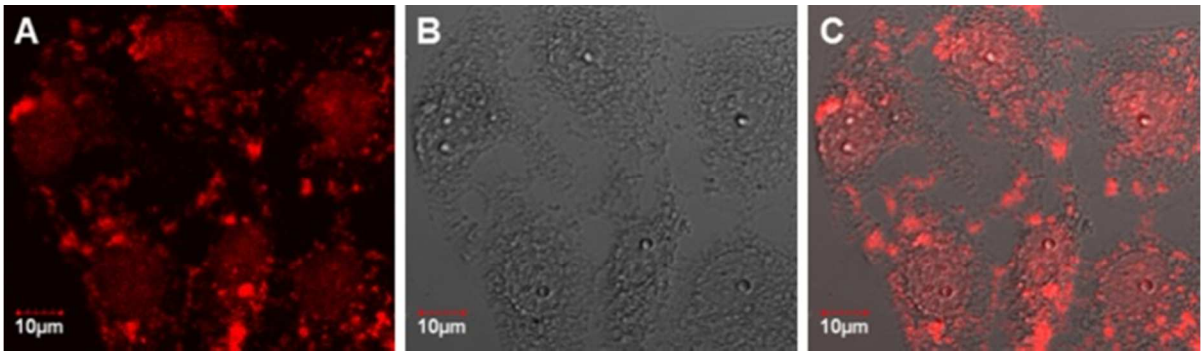

Figure 6. CLSM images of Hela cells after incubation with TPA-AN-TPM@Ps-PVPs (with a fluorogen loading of 10%)for 16 h at 37 °C. A: fluorescence image; B: bright field image; C: overlay of A and B.AIE dots Concentration: 0.15 mg/mL

the applications in biological imaging. The cytotoxicity of TPA-AN-TPM@Ps-PVPs in vitro against HeLa cells was investigated using a 3-(4,5-dimethylthiazol-2-yl)-2,5-diphenyltetrazolium bromide (MTT) cell-viability assay. Figure S5 shows the cell viability after incubation with the dots suspension at concentrations of 0.03, 0.15, and 0.3 mg/mL for 24 and 48 h, respectively. In the presence of TPA-AN-TPM@Ps-PVPs, HeLa cells grow similar as the control experiments (absence of TPA-AN-TPM@Ps-PVPs), indicating that the AIE dots have low cytotoxicity and are suitable for cell imaging.

The application of TPA-AN-TPM@Ps-PVPs for cellular imaging was studied using confocal laser scanning microscopy (CLSM). After incubation with the TPA-AN-TPM@Ps-PVPs suspension (0.15mg/mL) for 16 h at 37 °C in the culture medium, the HeLa cells were imaged by CLSM with a 405 nm laser excitation and the fluorescent signals were collected between 610 nm and 710 nm. As shown in Figure 6, an intense red fluorescence was observed in the cellular cytoplasm and nuclei.

TPA-AN-TPM@Ps-PVPs could stain cytoplasm of HeLa cells effectively and the intensive red fluorescence can be observed. However, it should be noted that the AIE dots possess ability to stain nuclei. Most of studies about living cells so far have concerned only with particle entry into the cytoplasm or the localization of receptors on the cell membrane. However, the nucleus is a much more desired target because the genetic information of the cell and transcription machinery reside there.[42] But the nuclear membrane is impermeable to most kinds of probes.[43-45]Developing novel nanoprobes for nuclei imaging would greatly favor the biological and biomedical research.

A possible mechanism of the uptake of TPA-AN-TPM@Ps-PVPs by nuclei was shown in Scheme S1. The outer layer pyridine salt of the nanoparticles carries positive charges. This pyridine salt is similar to the quaternary ammonium salt which has a high affinity with DNA which carries negative charges (binding constant ~ 105 M^{-1})[46]. Therefore, the surface of the dots could absorb DNA or RNA. Benefit from the small size at the same time, the dots could go along with DNA or RNA into the nuclei, when the genetic process was occurring.[43-45]

The above good properties make TPA-AN-TPM@Ps-PVPs promising for bioimaging applications.

Conclusions

We successfully synthesized an AIE molecule TPA-AN-TPM with the strategy "coating disc-like red emission fluorophores with propeller-shaped AIE fluorophores" and fabricated the ultrabright red AIE dots TPA-AN-TPM@Ps-PVPs by using luminogens with AIE feature as the core and biocompatible Ps-PVP as the encapsulation matrix. The AIE dots have spherical morphology, uniform small size, good stability in water and low cytotoxicity. The dots can stain both cytoplasm and nuclei and give a strong red fluorescence signal. It indicated that the kind of red AIE dots with high fluorescent quantum yield can be applied effectively in cytoplasm and nucleus imaging.

Experimental Section

Materials

All reagents and starting materials are commercially available and were used without further purification, unless otherwise noted. THF and 1, 4-dioxane was dried by distillation from sodium/benzophenone under nitrogen. PS-PVP was provided by State Key Laboratory of Luminescence and Applications, Changchun Institute of Optics.2-(2,6-bis((E)-2-(thiophen-2-yl)vinyl)-4H-pyran-4-ylidene)malononitrile (TPM), tetraethyl (anthracene-9,10- diylbis(methylene))bis(phosphonate) (1), 4-(diphenylamino)benzaldehyde (2), 4,4'-((4-bromophenyl)azanediyl)dibenzaldehyde (4), 2-(2,6-bis((E)-2-(5-bromothiophen-2-yl)vinyl)-4H-pyran-4-ylidene)malononitrile (6)were synthesized according to reference procedures.[47-50]

Instrumentations

^{1}H and ^{13}C NMR spectra were recorded on Bruker AVANVE 500 MHz spectrometer or Varian 300MHz with tetramethylsilane as the internal standard. Mass spectra were recorded using a Kratos MALDI-TOF mass system. UV-vis absorption spectra were recorded on a Shimadzu UV-3100 spectrophotometer. Photo luminescence spectra were collected

on a Shimadzu RF-5301PC spectrophotometer and Maya 2000Pro optical fiber spectrophotometer. Transmission electron microscopy (TEM) images were obtained with a transmission electron microscope (TEM, JEM2011). Zeta potentials and dynamic light scattering (DLS) measurements were performed using a Zeta Sizer instrument (Nano ZS, Malvern Instruments Ltd) at room temperature.

Measurements of fluorescence quantum yields

Solid state PL efficiencies were measured with an integrating sphere (C-701, Labsphere Inc.) with a 405 nm Ocean Optics LLS-LED as the excitation source, and the laser was introduced into the sphere through the optical fiber.

Fluorescence quantum yields for the solutions and suspensions were obtained by comparing to the fluorescence spectrum of rhodamine in ethanol (absorbance value < 0.1, excitation wavelength:365 nm, PL efficiencies Φ_r= 69%) with corrections of refractive index differences using eqn,[51, 52]

$$\Phi_s = \Phi_r \left(\frac{A_r}{A_s}\right)\left(\frac{I_s}{I_r}\right)\left(\frac{{n_s}^2}{{n_r}^2}\right)$$

Where Φ_r and Φ_s are the fluorescence quantum yields of standards and the samples, respectively. A_r and A_s are the absorbances of the standards and the measured samples at the excitation wavelength, respectively. I_r and I_s are the integrated emission intensities of standards and the samples. nr and ns are the refractive indices of the corresponding solvents of the solutions, respectively.

Synthesis of ((10-(4-(diphenylamino)styryl)anthracen-9-yl)methyl)phosphonate(3).

Compound 1 (2 g, 4.28 mmol) and compound 2 (1.09 g, 4 mmol) were dissolved in 40 mL of anhydrous THF. A solution of potassium tert-butoxide (493.72 mg, 4.4 mmol) in anhydrous THF (160 mL) was added drop wisely over a 6 h period at 0 ºC under nitrogen. The resultant mixture was allowed to warm to room temperature and then stirred 18 h. After solvent evaporation, 200 mL methanol was added. Then the mixture was sonicated, filtered and washed with methanol (50 mL × 3). The combined filtrate was concentrated by evaporation. Then the crude product was purified by silica gel chromatography (first CH_2Cl_2, then ethyl acetate) to give a yellow solid (1.15 g, 40% yield).^{1}H NMR (300 MHz, $CDCl_3$, δ),: 8.42-8.37 (t, 4H), 7.85-7.75 (d, J = 16.5Hz, 1H), 7.61-7.53 (t, 4H), 7.52-7.42 (t, 2H), 7.35-7.27 (t, 4H), 7.21-7.12 (m, 6H), 7.10-7.02 (t, 2H), 6.88-6.79 (d, J =1 6.5Hz, 1H), 4.32-4.20 (d, 2H), 4.00-3.78 (m, 4H), 1.15-1.07 (m, 6H) ; ^{13}C NMR ($CDCl_3$, 75 MHz), δ (TMS, ppm): 147.82, 146.62, 137.06, 131.48, 130.37, 129.74, 129.47, 127.57, 126.96, 125.77, 125.00, 124.59, 123.78, 123.24.

Synthesis of 4-bromo-N, N-bis(4-((E)-2-(10-((E)-4-(diphenylamino)styryl)anthracen-9-yl)vinyl)phenyl) aniline (TPA-AN-B)

Compound 3 (1.37 g, 2.2mmol) and potassium tert-butoxide (0.38 g, 3.3mmol) were dissolved in anhydrous THF (150 mL). A solution of compound 4 (0.40, 1 mmol) in anhydrous THF (40 mL) was added drop wisely over a 20 min period at 0 ºC under nitrogen. The resultant mixture was allowed to warm to room temperature and then stirred 24 h. After solvent evaporation, 200 mL methanol was added. Then the mixture was sonicated, filtered and washed with methanol (50 mL × 3). The residue was purified by silica gel chromatography (CH_2Cl_2) to give a yellow solid (0.76 g, 60% yield). ^{1}H NMR ($CDCl_3$, 300 MHz), δ (TMS, ppm): 8.49-8.36 (m, 8H), 7.89 (d, J = 16.5Hz, 2H), 7.84 (d, J = 16.5Hz, 2H), 7.67-7.54 (m, 8H), 7.54-7.46 (m, 8H), 7.46-7.40 (m, 2H), 7.36-7.29 (m, 10H), 7.26-7.23 (d, 2H,), 7.20-7.15 (m, 14), 7.12-7.04 (t, 4H), 6.92 (d, J = 16.5Hz, 2H), 6.90 (d, J = 16.5Hz, 2H); ^{13}C NMR ($CDCl_3$, 75 MHz), δ (TMS, ppm): 147.68, 147.52, 136.87, 134.04, 132.43, 131.42, 129.56, 129.29, 127.60, 127.41, 126.51, 125.72, 125.12, 124.46, 123.67, 123.05; MALDI-TOF MS: $C_{90}H_{64}BrN_3$ (M+H), calcd. 1265.43; found 1267.

Synthesis of N,N-bis(4-((E)-2-(10-((E)-4-(diphenylamino) styryl)anthracen-9-yl)vinyl)phenyl)-N-(4-(4,4,5,5-tetramethyl-1,3,2-dioxaborolan-2-yl)phenyl)aniline(5)

Bis(pinacolato)diboron (380 mg,1.5 mmol), potassium acetate (390 mg, 4 mmol), [1,1'-bis(diphenylphosphino)ferrocene] dichloropalladium(II) (12 mg,0.015 mol) and TPA-AN-Br (1.267 g,1 mmol) were dissolved in distilled 1,4 -dioxane (30 mL). The mixture was stirred at 80 ºC for 8 h under nitrogen. After being cooled to room temperature, the reaction mixture was poured into water (100 mL) and extracted with CH_2Cl_2 (150 mL× 3). The combined organic extracts were washed with brine, dried over $MgSO_4$, and concentrated to dryness under vacuum. The crude product was purified by silica gel chromatography (CH_2Cl_2) to give an orange solid (0.96g, 69%yield). ^{1}H NMR ($CDCl_3$,300 MHz), δ(TMS, ppm): 8.45-8.40 (m, 8H), 7.88 (d, J =16.5Hz, 2H), 7.82 (d, J =16.5Hz, 2H), 7.79-7.76 (d, 2H), 7.65-7.54 (m, 8H), 7.52-7.45 (m, 8H), 7.34-7.27 (m, 10H), 7.25-7.23 (d, 2H), 7.21-7.13 (m, 14H), 7.10-7.02 (m, 4H), 6.93 (d, J =16.5Hz, 2H), 6.88 (d, J =16.5Hz, 2H); ^{13}C NMR ($CDCl_3$, 75 MHz), δ (TMS, ppm):147.64, 147.50, 146.89, 136.79, 136.05, 132.53, 131.45, 129.55, 129.28, 127.40, 126.49, 125.11, 124.85, 124.45, 123.68, 123.04, 122.56, 83.62, 24.85; MALDI-TOF MS: $C_{96}H_{76}BN_3O_2$ (M+H), calcd. 1314.61; found 1314.

Synthesis of 2-(2,6-bis((E)-2-(5-(N,N-bis(4-((E)-2-(10-((E)-4-(diphenylamino)styryl)anthracen-9-yl)vinyl)phenyl)aniline-4-yl)thiophen-2-yl)vinyl)-4H-pyran-4-ylidene)malononitrile (TPA-AN-TPM)

Compound 5 (262 mg, 0.2 mmol), Compound 6 (51 mg, 0.1 mmol) and tetrakis(triphenylphosphine)palladium (9.2 mg, 0.008 mmol) were placed in a flask under nitrogen. Then toluene (15 mL) and Na_2CO_3 aqueous solution (2M, 10 mL) were added into the mixture and stirred at 110 ºC for 48 h. After being cooled to room temperature, the reaction mixture was poured into water (50 mL) and extracted with CH_2Cl_2 (100 mL× 3). The combined organic extracts were dried over $MgSO_4$ and concentrated to dryness under vacuum. The crude product was purified by silica gel chromatography (CH_2Cl_2) to give a black-red solid (0.15g, 56% yield).^{1}H NMR (CDCl3, 500 MHz),δ(TMS, ppm): 8.55-8.29 (m, 16H), 7.95-7.88 (d, J =

16.5Hz, 4H), 7.86-7.81 (d, J = 16.5Hz, 4H), 7.76-7.74 (m, 2H), 7.71-7.64 (d, 6H), 7.64-7.57 (m, 12H), 7.57-7.43 (m, 22H), 7.40-7.31 (m,24H), 7.24-7.17 (m, 20H), 7.16-7.14 (m, 2H), 7.11-7.08 (t, 8H), 7.00-6.94 (d, J = 16.5Hz, 4H), 6.93-6.88 (d, J = 16.5Hz, 4H), 6.64-6.63 (s, 2H), 6.59-6.53 (d, J = 16.5Hz, 2H), 6.53-6.49 (d, J = 16.5Hz, 2H); ^{13}C NMR (CDCl3, 75 MHz), δ (TMS, ppm): 147.58, 136.96, 132.97, 132.46, 131.31, 130.82, 129.66, 129.30, 128.81, 127.73, 127.44, 126.96, 126.58, 126.40, 125.19, 124.94, 124.54, 123.70, 123.31, 123.11, 121.65, 116.48, 115.18, 103.98, 65.50; MALDI-TOF MS: $C_{200}H_{138}N_8OS_2$ (M+H), calcd. 2733.05; found 2733.221.

Fabrication of TPA-AN-TPM@PS-PVP Dots

TPA-AN-TPM@PS-PVP dots with varied loading ratios of TPA-AN-TPM ranging from 1 to 10wt% were prepared. The preparation of the dots with a fluorogen loading of 10 wt% was given as a representative. In brief, 10 mg PS-PVP was dissolved in 0.5 THF. Subsequently, 0.25 mL THF solution containing 1mg TPA-AN-TPM was added and stirred for 0.5 h. Then 5 mL hydrochloric acid (pH = 2) was injected into the solution at a rate of 0.5 mL h^{-1}. After that, the suspension was dialyzed by hydrochloric acid (PH = 4) 3 times (250 mL and 24 h for each time). Then the suspension was filtered through a 0.45 μm micro filter and sealed before use. AIE dots with varied loading ratios of TPA-AN-TPM were obtained by converting the starting ratio of TPA-AN-TPM and PS-PVP.

Cell culture

HeLa cells were cultured in minimum essential medium containing 10% fetal bovine serum and antibiotics (100 units per mL penicillin and 100 mg/mL streptomycin) in a 5% carbon dioxide humidity incubator at 37 ºC. The cell proliferation Kit I (MTT) was used to measure the cell viability. First, 500 cells were seeded per well in a 96-well plate. After overnight culture, various concentrations of TPA-AN-TPM@PS-PVP dots were added into the 96-well plate. After 12 h, 24 h, 48 h. 10 mL of MTT solution (5 mg mL-1 in PBS) was added into each well. After 4 h incubation at 37 ºC, 100 mL of solubilization mixture containing 10% SDS and 0.01 M HCl was added to dissolve the purple crystals. After 12 h, the absorbance was measured at 590 nm. Every experiment was performed at least three times.

Cell imaging

HeLa cells were grown overnight in a 20 mm Petri dish. The living cells were stained with TPA-AN-TPM@PS-PVP dots with a final concentration of 0.15 mg mL^{-1} and incubated for 16 h. The cells were imaged under an inverted confocal laser scanning microscopy (Olympus, FV1000; λ_{ex} = 405 nm fluorescent signals were collected at 610–710 nm). The images of the cells were captured using a photomultiplier.

Acknowledgements

This work was supported by 973 Program (2013CB834702), the Natural Science Foundation of China(No. 51373063, 21204027, 21221063), and the Project of Jilin Province (20100704).

Notes and references

1. V. Ntziachristos, *Annu. Rev. Biomed. Eng.*, 2006, 8, 1-33.
2. Y. Wang, C. Xu and H. Ow, *Theranostics*, 2013, 3, 544.
3. Y.-S. Lin, N. Abadeer, K. R. Hurley and C. L. Haynes, *Journal of the American Chemical Society*, 2011, 133, 20444-20457.
4. W. C. Chan and S. Nie, *Science*, 1998, 281, 2016-2018.
5. L. R. Hirsch, A. M. Gobin, A. R. Lowery, F. Tam, R. A. Drezek, N. J. Halas and J. L. West, *Annals of Biomedical Engineering*, 2006, 34, 15-22.
6. J. S. Hrkach, M. T. Peracchia, A. Bomb and R. Langer, *Biomaterials*, 1997, 18, 27-30.
7. K. Li, W. Qin, D. Ding, N. Tomczak, J. Geng, R. Liu, J. Liu, X. Zhang, H. Liu and B. Liu, *Scientific reports*, 2013, 3.
8. R. Alford, H. M. Simpson, J. Duberman, G. C. Hill, M. Ogawa, C. Regino, H. Kobayashi and P. L. Choyke, *Molecular imaging*, 2009, 8, 341-354.
9. J. B. Birks, *Photophysics of aromatic molecules*, Wiley, New York, 1970.
10. W. Jacky, H. SingáKwok and B. ZhongáTang, *Chemical Communications*, 2001, 1740-1741.
11. H. Li, J. Mei, J. Wang, S. Zhang, Q. Zhao, Q. Wei, A. Qin, J. Sun and B. Z. Tang, *Science China Chemistry*, 2011, 54, 611-616.
12. V. R. Kondepati, H. M. Heise and J. Backhaus, *Analytical and bioanalytical chemistry*, 2008, 390, 125-139.
13. S. Luo, E. Zhang, Y. Su, T. Cheng and C. Shi, *Biomaterials*, 2011, 32, 7127-7138.
14. 钱立军, 支俊格, 佟斌, 杨帆, 赵玮 and 董宇平, *化学进展*, 2008, 20, 673-678.
15. 张双, 秦安军, 孙景志 and 唐本忠, *化学进展*, 2011, 23, 623-636.
16. Y. Hong, M. Häuβler, J. W. Lam, Z. Li, K. K. Sin, Y. Dong, H. Tong, J. Liu, A. Qin and R. Renneberg, *Chemistry-A European Journal*, 2008, 14, 6428-6437.
17. J. Geng, K. Li, D. Ding, X. Zhang, W. Qin, J. Liu, B. Z. Tang and B. Liu, *Small*, 2012, 8, 3655-3663.
18. Y. Hong, J. W. Lam and B. Z. Tang, *Chemical Communications*, 2009, 4332-4353.
19. 闫继明, 秦安军, 孙景志 and 唐本忠, *科学通报*, 2010, 1206-1213.
20. 董永强 and 唐本忠, *激光与光电子学进展*, 2008, 23-23.
21. Z. Zhao, J. Geng, Z. Chang, S. Chen, C. Deng, T. Jiang, W. Qin, J. W. Y. Lam, H. S. Kwok, H. Qiu, B. Liu and B. Z. Tang, *Journal of Materials Chemistry*, 2012, 22, 11018-11021.
22. G. Qian, B. Dai, M. Luo, D. Yu, J. Zhan, Z. Zhang, D. Ma and Z. Y. Wang, *Chemistry of Materials*, 2008, 20, 6208-6216.
23. X. Li, B. Xu, H. Lu, Z. Wang, J. Zhang, Y. Zhang, Y. Dong, K. Ma, S. Wen and W. Tian, *Analytical Methods*, 2013, 5, 438-441.
24. W. Qin, D. Ding, J. Liu, W. Z. Yuan, Y. Hu, B. Liu and B. Z. Tang, *Advanced Functional Materials*, 2012, 22, 771-779.
25. J. Geng, K. Li, W. Qin, L. Ma, G. G. Gurzadyan, B. Z. Tang and B. Liu, *Small*, 2013, 9, 2012-2019.
26. H. Shi, N. Zhao, D. Ding, J. Liang, B. Z. Tang and B. Liu, *Organic & biomolecular chemistry*, 2013, 11, 7289-7296.

27. 夏晶, 吴燕梅, 张亚玲, 佟斌, 石建兵, 支俊格 and 董宇平, *影像科学与光化学*, 2012, 30, 9-25.
28. Y. Hong, J. W. Lam and B. Z. Tang, *Chemical Society Reviews*, 2011, 40, 5361-5388.
29. M. A. Wolak, J. Delcamp, C. A. Landis, P. A. Lane, J. Anthony and Z. Kafafi, *Advanced Functional Materials*, 2006, 16, 1943-1949.
30. F. Nüesch, D. Berner, E. Tutiš, M. Schaer, C. Ma, X. Wang, B. Zhang and L. Zuppiroli, *Advanced Functional Materials*, 2005, 15, 323-330.
31. G. Ulrich, R. Ziessel and A. Harriman, *Angewandte Chemie International Edition*, 2008, 47, 1184-1201.
32. Z. Zhao, J. Geng, Z. Chang, S. Chen, C. Deng, T. Jiang, W. Qin, J. W. Lam, H. S. Kwok and H. Qiu, *Journal of Materials Chemistry*, 2012, 22, 11018-11021.
33. W. Qin, D. Ding, J. Liu, W. Z. Yuan, Y. Hu, B. Liu and B. Z. Tang, *Advanced Functional Materials*, 2012, 22, 771-779.
34. B.-j. Xu, Z.-g. Chi, X.-f. Li, H.-y. Li, W. Zhou, X.-q. Zhang, C.-c. Wang, Y. Zhang, S.-w. Liu and J.-r. Xu, *Journal of fluorescence*, 2011, 21, 433-441.
35. H. Li, Z. Chi, X. Zhang, B. Xu, S. Liu, Y. Zhang and J. Xu, *Chemical Communications*, 2011, 47, 11273-11275.
36. B. Xu, H. Fang, Y. Dong, F. Chen, Q. Chen, H. Sun and W. Tian, *New J. Chem.*, 2010, 34, 1838-1842.
37. 徐斌, 张继博, 马愫倩, 陈金龙, 董玉杰 and 田文晶*, *化学进展*, 2013, 25, 1079-1089.
38. J. Zhang, B. Xu, J. Chen, S. Ma, Y. Dong, L. Wang, B. Li, L. Ye and W. Tian, *Adv. Mater.*, 2013.
39. L. Wang, B. Xu, J. Zhang, Y. Dong, S. Wen, H. Zhang and W. Tian, *Physical Chemistry Chemical Physics*, 2013, 15, 2449-2458.
40. J. He, B. Xu, F. Chen, H. Xia, K. Li, L. Ye and W. Tian, *The Journal of Physical Chemistry C*, 2009, 113, 9892-9899.
41. C.-K. Lim, S. Kim, I. C. Kwon, C.-H. Ahn and S. Y. Park, *Chemistry of Materials*, 2009, 21, 5819-5825.
42. S. Nakielny and G. Dreyfuss, *Cell*, 1999, 99, 677-690.
43. J.-n. Liu, W. Bu, L.-m. Pan, S. Zhang, F. Chen, L. Zhou, K.-l. Zhao, W. Peng and J. Shi, *Biomaterials*, 2012.
44. M. M. Gottesman, T. Fojo and S. E. Bates, *Nature Reviews Cancer*, 2002, 2, 48-58.
45. B. Kang, M. A. Mackey and M. A. El-Sayed, *Journal of the American Chemical Society*, 2010, 132, 1517-1519.
46. W. Zhong, J. S. Yu, W. Huang, K. Ni and Y. Liang, *Biopolymers*, 2001, 62, 315-323.
47. H. Lu, F. Su, Q. Mei, X. Zhou, Y. Tian, W. Tian, R. H. Johnson and D. R. Meldrum, *Journal of Polymer Science Part A: Polymer Chemistry*, 2012, 50, 890-899.
48. W. Xu, B. Peng, J. Chen, M. Liang and F. Cai, *The Journal of Physical Chemistry C*, 2008, 112, 874-880.
49. J. Sirotkina, L. Laipniece, K. Lazdovica, B. Turovska and V. Kampars, *Scientific Proceedings of Riga Technical University, Series 1: Material Science and Applied Chemistry*, 2012, 25, 2012.
50. M. Vanjinathan, H.-C. Lin and A. S. Nasar, *Journal of Polymer Science Part A: Polymer Chemistry*, 2012, 50, 3806-3818.
51. J. Burroughes, D. Bradley, A. Brown, R. Marks, K. Mackay, R. Friend, P. Burns and A. Holmes, *nature*, 1990, 347, 539-541.
52. S. R. Forrest, *Nature*, 2004, 428, 911-918.

a State Key Laboratory of Supramolecular Structure and Materials, Jilin University,Changchun, 130012, P. R. China.
b Edmond H. Fischer Signal Transduction Laboratory, College of Life Sciences, Jilin University, Changchun 130023, P. R. China
c State Key Laboratory of Luminescence and Applications, Changchun Institute of Optics, Fine Mechanics and Physics, Chinese Academy of Sciences, Changchun, 130033, P. R. China.

Electronic Supplementary Information (ESI) available: See DOI: 10.1039/b000000x/

